
ACCELERATING RANS TURBULENCE MODELING USING POTENTIAL FLOW AND MACHINE LEARNING

A PREPRINT

Romit Maulik

Argonne Leadership Computing Facility
Argonne National Laboratory
Lemont, IL 60439
rmaulik@anl.gov

Himanshu Sharma

Argonne Leadership Computing Facility
Argonne National Laboratory
Lemont, IL 60439
hsharma@anl.gov

Saumil Patel

Computational Science Division
Argonne National Laboratory
Lemont, IL 60439
hsharma@anl.gov

Bethany Lusch

Argonne Leadership Computing Facility
Argonne National Laboratory
Lemont, IL 60439
blusch@anl.gov

Elise Jennings

Argonne Leadership Computing Facility
Argonne National Laboratory
Lemont, IL 60439
ejennings@anl.gov

October 11, 2024

ABSTRACT

Reynolds-averaged Navier-Stokes (RANS) equations for steady-state assessment of incompressible turbulent flows remain the workhorse for practical computational fluid dynamics (CFD) applications, and improvements in speed or accuracy have the potential to affect a diverse range of sectors. We introduce a machine learning framework for the acceleration of RANS by training an artificial neural network to predict steady-state turbulent eddy viscosities. This surrogate model for the turbulent eddy viscosity is assessed for parametric interpolation, while solving for the pressure and velocity equations to steady state, thus representing a framework that is hybridized with machine learning. We achieve accurate steady-state results with significant reduction in solution time when compared to those obtained by the Spalart-Allmaras one-equation model. Most notably the proposed methodology allows for considerably larger relaxation factors for the steady-state velocity and pressure solvers. Our assessments are made for a backward-facing step with considerable mesh anisotropy and separation to represent a practical CFD application. For two test experiments with different inlet velocity conditions we see a factor of 6.8 and 7.5 decrease in the overall time to convergence. The proposed framework represents an excellent opportunity for rapid exploration of large parameter spaces which prove prohibitive when utilizing turbulence closure models with extra coupled partial differential equations.

1 Introduction

The direct numerical simulation (DNS) of turbulence is impractical for most applications due to its multiscale nature. Engineering decisions requiring short turnover durations continue to rely on the Reynolds-averaged Navier-Stokes (RANS) equations for steady-state analysis of turbulent flows. Within that context, developments that lead to improved RANS results from the point of view of speed or accuracy have the potential to affect design workflows significantly. To that end, there have been several recent investigations into the augmentation of RANS using data-driven methods that

attempt to improve its accuracy through the use of fidelity porting strategies [1, 2, 3] or the utilization of experimental data [4]. Closure optimization strategies have also looked at zonal coefficient refinement or model selection for improved accuracy [5, 6]. Most attempts at infusing information from higher fidelity models such as DNS to reduced-order representations have resulted in improved accuracy for the quantities of interest and represent the bulk of physics-informed machine learning investigations of turbulence closure modeling [7, 8, 9, 10]. The numerous opportunities for utilizing machine learning in turbulence modeling have been summarized recently in a review by [11].

In contrast to most investigations of closure modeling using machine learning, a recent investigation [12] has looked at the surrogate modeling of subsonic flow around an airfoil with a radial-basis function network. The unique feature of this study was a section devoted to the improvements in compute time due to the preclusion of a separate partial differential equation (PDE) for the turbulent eddy viscosity computation. Similarly, this article investigates an alternate route to RANS acceleration through the direct construction of steady-state turbulent eddy viscosity fields with the use of a deep learning framework. We leverage potential flow solutions of our test case across a range of boundary conditions as inputs and harvest steady-state turbulent eddy viscosities (from a suitable choice of a turbulence closure model based on the linear eddy-viscosity hypothesis) as outputs to train a relationship which can be deployed solely *once* at the start of a RANS simulation. The velocity and pressure equations are solved to steady-state while utilizing this *fixed* solution. It is observed that the resultant RANS solutions are as accurate as those obtained by the PDE model but with the added advantage of significant reductions to the total time-to-solution. In addition, sampling of the control parameter space also allows for interpolation using the proposed surrogate closure.

The machine learning (ML) framework presented here consists of two phases, which we refer to as *offline* and *online*. The offline phase consists of data generation at strategically selected points in parameter space (corresponding to a design of experiments component) as well as the training of a neural network to predict a turbulent eddy-viscosity. This trained network is the ML surrogate model. The online phase corresponds to the deployment of the trained ML surrogate to predict a spatial field of eddy-viscosities which are then held fixed, while the velocity and pressure equations are solved to convergence. The overall procedure with online and offline phases for training and deploying the ML surrogate is denoted “the machine learning framework.” Crucially, our test case is given by the two-dimensional backward-facing step exhibiting flow separation and considerable mesh anisotropy and thus represents a challenging test for the construction of surrogate closures for real-world applications. We note that the mesh utilized in this study, which will be introduced in greater detail in Section 2.1, is from the NASA LARC extended turbulence validation database.

2 Methodology

This section describes the proposed data-driven workflow and test case. In subsections 2.1 and 2.2 we define the problem statement and provide a brief background of RANS modeling. In subsection 2.3 a description of the proposed machine learning (ML) and computational fluid dynamics (ML-CFD) integration procedure is provided.

2.1 Problem Definition

In the current work, we undertake the problem of simulating flow past the backward-facing step as shown in figure 1(a). The experimental description is provided in [13]. We simulate the airflow for a Reynolds number based on the step height of $h = 1.27$ cm. The Reynolds number is defined as $Re_h = \frac{Uh}{\nu}$ where U is the free-stream velocity (and also a control parameter for generating training and testing data in our machine learning problem definition) and $\nu = 1.5 \times 10^{-5} \frac{m^2}{s}$ is the kinematic viscosity. The problem is widely used for the validation of novel turbulence models. More details about the case can be seen on the NASA turbulence web page¹.

The training data set is generated from ten simulations, each with distinct free-stream velocities resulting in Reynolds numbers that range from $Re_h = 34,000$ - $41,500$. All CFD simulations are performed with the OpenFOAM solver (version 5.0) [14] which has seen extensive use in practical CFD applications [15]. The computational domain is composed of a non-uniform grid as shown in figure 1. To capture the separation occurring near the step, additional refinement was performed on the grid, which can be seen in the zoomed view shown in figure 1(b). The total number of cells used in the study was fixed at 20,540. The mesh was generated using OpenFOAM’s native grid generator `blockMesh`, with a maximum aspect ratio of 7,601.12. The grid is used to generate the potential flow solution, the need for which will be explained in subsection 2.3 outlining the ML-CFD integration.

¹https://turbmodels.larc.nasa.gov/backstep_val.html

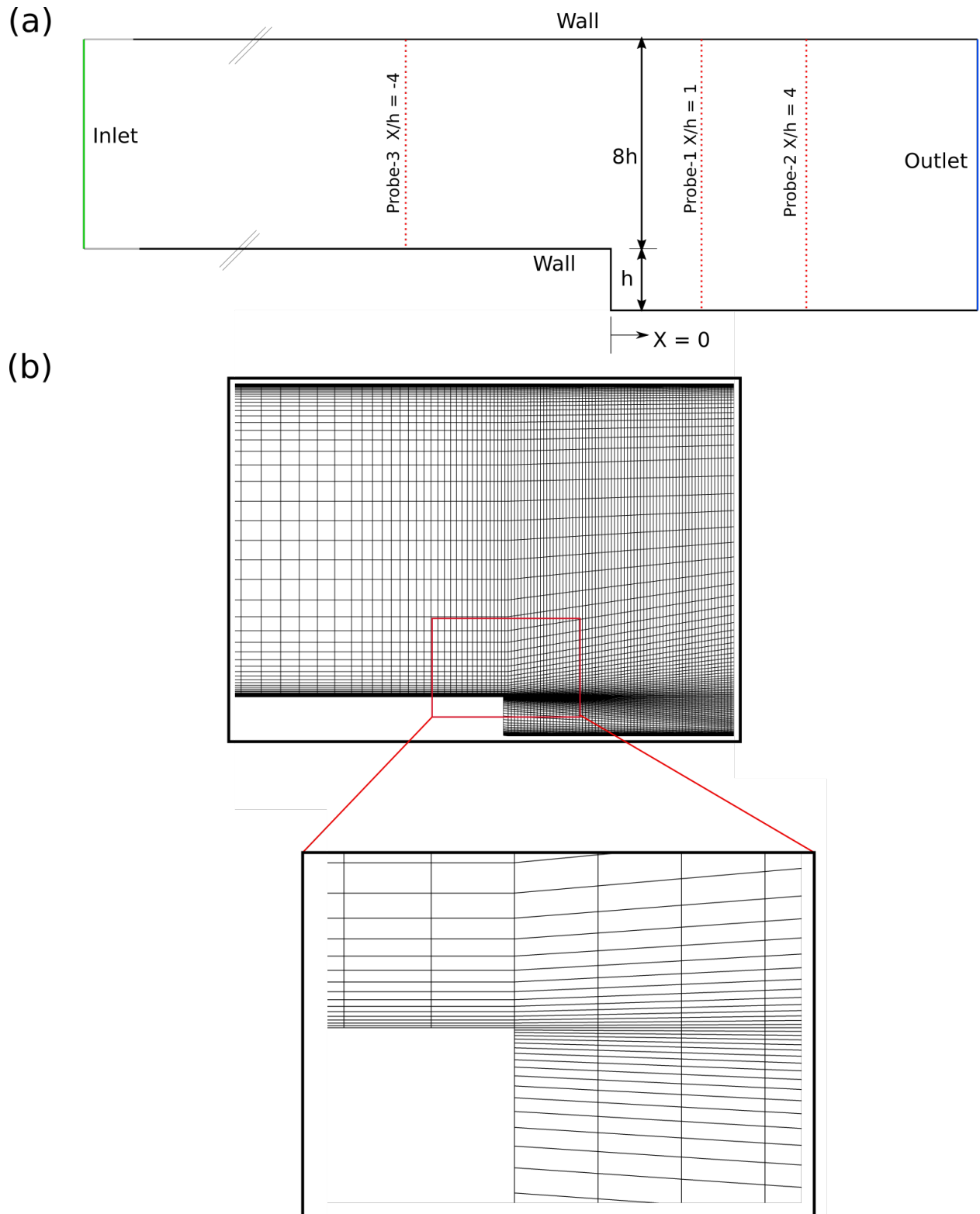


Figure 1: The backward step used for carrying CFD simulation. (a) shows the geometry and the step defined at $(0,0)$. Red dash lines show locations where data has been probed to assess our ML surrogate model. (b) shows the mesh used for the computation. (c) shows the zoomed view of the refined mesh.

2.2 RANS

The RANS equations are a time-averaged form of the Navier-Stokes equations of motion for fluid flow. The equations are derived using the Reynolds decomposition principle shown in [16], whereby the instantaneous quantity is decomposed into its time-averaged and fluctuating quantities. These equations are used for describing the steady-state behavior of turbulent flows. In Cartesian coordinates for a stationary flow of an incompressible Newtonian fluid, the RANS equations can be written as follows:

$$\frac{\partial \bar{u}_i}{\partial x_i} = 0, \quad (1a)$$

$$\rho \bar{u}_j \frac{\partial \bar{u}_i}{\partial x_j} = \rho \bar{f}_i + \frac{\partial}{\partial x_j} \left[-\bar{p} \delta_{ij} + 2\mu \bar{S}_{ij} - \overline{\rho u'_i u'_j} \right] \quad (1b)$$

where $\bar{\cdot}$ denotes time-averaged quantities, u is the velocity component, u' is the fluctuating component, p is the pressure, ρ is the density of fluid, f_i is a vector representing external forces, δ_{ij} is the Kronecker delta function, μ is the dynamic viscosity, and $\bar{S}_{ij} = \frac{1}{2} \left(\frac{\partial \bar{u}_i}{\partial x_j} + \frac{\partial \bar{u}_j}{\partial x_i} \right)$ is the mean rate of the stress tensor. The left-hand side of this equation defines the change of the mean momentum of the fluid element due to the unsteadiness of the mean flow and the convection. The change is balanced by the mean body force, the isotropic stress resulting from the mean pressure field, the viscous stresses and the stresses $(-\overline{\rho u'_i u'_j})$ due to the fluctuating velocity field, generally denoted the *Reynolds stress*. This nonlinear term requires an additional model specification to close the RANS equation. Most methods deal with an explicit model for this tensor through the utilization of additional algebraic or differential equations. Some of these are based on the time evolution of the Reynolds stress equation as presented in [17]. The bulk of our experiments in this investigation utilizes the one-equation Spalart-Allmaras [18] model (SA) for the generation of reference data sets. The SA model closure is written in the following form:

$$\begin{aligned} \frac{\partial \tilde{\nu}}{\partial t} + u_j \frac{\partial \tilde{\nu}}{\partial x_j} &= C_{b1} [1 - f_{t2}] \tilde{S} \tilde{\nu} + \frac{1}{\sigma} \{ \nabla \cdot [(\nu + \tilde{\nu}) \nabla \tilde{\nu}] + C_{b2} |\nabla \tilde{\nu}|^2 \} \\ &- \left[C_{w1} f_w - \frac{C_{b1}}{\kappa^2} f_{t2} \right] \left(\frac{\tilde{\nu}}{d} \right)^2 + f_{t1} \Delta U^2 \end{aligned} \quad (2)$$

where turbulent eddy viscosity is defined as $\nu_t = \tilde{\nu} f_{v1}$, $f_{v1} = \frac{\chi^3}{\chi^3 + C_{v1}^3}$, $\chi := \frac{\tilde{\nu}}{\nu}$, $\tilde{S} \equiv S + \frac{\tilde{\nu}}{\kappa^2 d^2} f_{v2}$, $f_{v2} = 1 - \frac{\chi}{1 + \chi f_{v1}}$, $f_w = g \left[\frac{1 + C_{w3}}{g^6 + C_{w3}^6} \right]^{1/6}$, $g = r + C_{w2}(r^6 - r)$, $r \equiv \frac{\tilde{\nu}}{S \kappa^2 d^2}$, $f_{t1} = C_{t1} g_t \exp(-C_{t2} \frac{\omega_t^2}{\Delta U^2} [d^2 + g_t^2 d_t^2])$, $f_{t2} = C_{t3} \exp(-C_{t4} \chi^2)$, $S = \sqrt{2 \Omega_{ij} \Omega_{ij}}$, the rotation tensor is given by $\Omega_{ij} = \frac{1}{2} (\partial u_i / \partial x_j - \partial u_j / \partial x_i)$, d is the distance from the closest surface and ΔU^2 is the norm of the difference between the velocity, $\sigma = 2/3$, $C_{b1} = 0.1355$, $C_{b2} = 0.622$, $\kappa = 0.41$, $C_{w1} = C_{b1} / \kappa^2 + (1 + C_{b2}) / \sigma$, $C_{w2} = 0.3$, $C_{w3} = 2$, $C_{v1} = 7.1$, $C_{t1} = 1$, $C_{t2} = 2$, $C_{t3} = 1.1$, $C_{t4} = 2$. The model defines a transport equation for a new viscosity-like variable $\tilde{\nu}$. To solve the SA equation for the turbulence closure of RANS, the following boundary conditions are prescribed; at wall $\tilde{\nu} = 0$, freestream/inlet $\tilde{\nu} = 3\nu$ and outlets are defined with Neumann condition. In the present work we use the SA closure to generate the steady state field of ν_t by solving the RANS equation, which is used as training data for the developing machine learning model. In addition, we also utilize the two-equation RNG $k - \epsilon$ [19] and $k - \omega$ SST [20] models for demonstrating the generality of the proposed framework. These model equations are widely used for a variety of practical turbulence modeling applications for simulating complex flows. We also generate the steady state ν_t field using these models. The equations for these models are omitted here for brevity but correspond to Eqs. (4.35), (4.42) and (5.10) for RNG $k - \epsilon$ in [19] and Eqs. A1-2, A13-15 for $k - \omega$ SST in [20].

Using OpenFOAM-based nomenclature, Table 1 provides a summary of the boundary conditions for each closure model employed during the data-generation phase of our workflow.

Once our governing equations are formulated, they must be solved on a discrete grid. We utilize the finite-volume method to ensure local conservation of our governing laws. This method requires the numerical calculation of spatial gradients for which we use a second-order accurate discretization. In particular, our viscous terms use a purely central discretization, whereas the advective terms use the LUST (blended linear and linear upwind scheme) to control for any spurious Gibbs phenomena. We note that these discretization methods are commonly used in practical CFD applications. Our problem utilizes a steady-state solver given by the SIMPLE algorithm. Our finite volume solver and machine learning deployment framework are built on a modified version of OpenFOAM 5.0 into which the C-backend of Tensorflow 1.14 [21] has been integrated. We note that both software are open-source.

OpenFOAM Boundary Conditions

SA			
Boundary Type	ν_t	$\tilde{\nu}$	
Inlet	calculated	3ν	
Outlet	calculated	zeroGradient	
Wall	fixedValue= 0.0	0.0	

$k - \omega$ SST			
Boundary Type	k	ω	ν_t
Inlet	fixedValue	fixedValue	calculated
Outlet	zeroGradient	zeroGradient	calculated
Wall	kqRwallFunction	omegaWallFunction	nutUSpaldingWallFunction

$k - \epsilon$ RNG			
Boundary Type	k	ϵ	ν_t
Inlet	fixedValue	fixedValue	calculated
Outlet	zeroGradient	zeroGradient	calculated
Wall	kqRwallFunction	epsilonWallFunction	fixedValue=0.0

Table 1: OpenFOAM-based nomenclature to describe the boundary conditions for each turbulence model employed in this study.

2.3 ML-RANS Integration

The core idea behind this investigation motivates the development of a surrogate turbulent-eddy viscosity model to bypass the solution of any extra equations for closure. While the previous section has introduced the SA equation as our reference model, we note that models of any fidelity can be used to generate the data needed by the framework. This shall also be demonstrated on two examples of two-equation models below. The core procedure is given below:

1. Data generation phase

- Select numerical experiment locations in the design space. In our study, this corresponds to different boundary conditions for inlet velocity.
- Initialize initial conditions for numerical experiments using potential flow solutions.
- Generate steady-state turbulent eddy-viscosity profiles using an *a priori* specified closure model (in this case SA).
- Augment initial condition information through feature preprocessing or geometric information embedding (for instance distance from the wall).
- Save training data in the form of pointwise input-output pairs of initial conditions and steady-state turbulent eddy viscosities.

2. Training phase

- Train an ML surrogate to predict pointwise steady-state turbulent eddy viscosities given initial conditions (i.e., potential flow solutions) as input.
- Train framework using 90% of the total data set, referred to as the training data; keeping the rest (10%) as validation data for model selection and to detect any potential overfitting of the model.
- Save the trained model for deployment.

3. Testing phase

- Choose a new design point in experiment space, for instance, a new value for inlet velocity.
- Generate initial conditions for this new point using potential flow - these will be the *test* inputs to the trained framework.
- Deploy the previously trained framework to predict an approximation for the steady-state turbulent eddy viscosity and fix this quantity permanently.
- Solve the Reynolds-averaged pressure and velocity equations to steady-state while utilizing the fixed steady-state turbulent eddy viscosity.

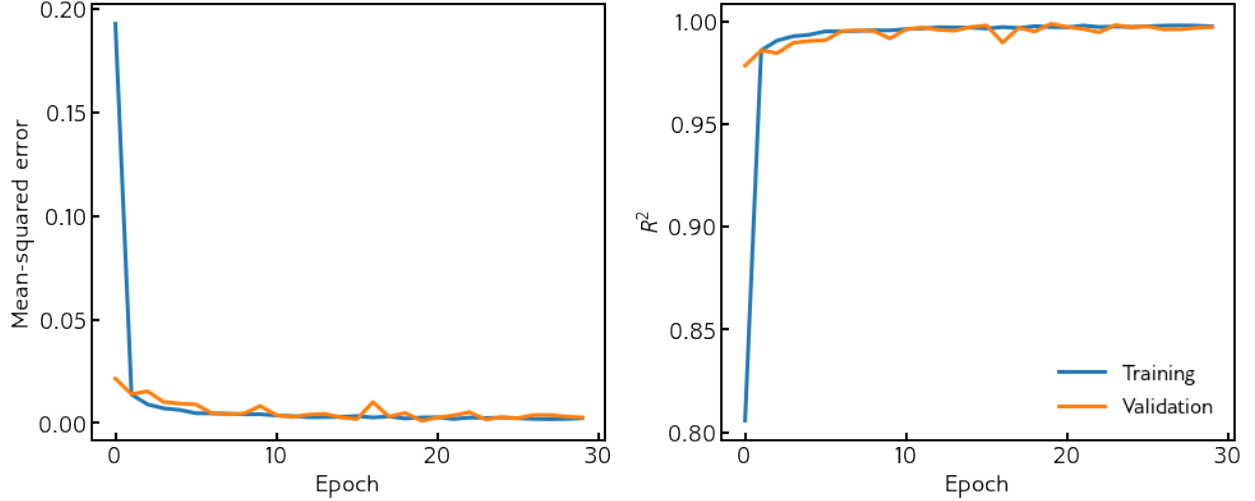


Figure 2: Progress to convergence for our deep learning architecture.

- Assess the impact of the surrogate eddy viscosity through quantitative metrics.

We now proceed with a tabulation of our input and output features in this study. Our inputs identify the region in space for model deployment through inputs of the finite-volume cell-centered coordinates and the initial conditions given by a potential flow solution. We note that our inputs and outputs were scaled to having unit mean and zero variance for each feature to enable easier training. Therefore our ML surrogate is given by

$$\mathbb{M} : u^p(\mathbf{x}), v^p(\mathbf{x}), x^c(\mathbf{x}), y^c(\mathbf{x}) \rightarrow \nu_t(\mathbf{x}) \quad (3)$$

where u^p and v^p indicate the horizontal and vertical velocities resulting from the potential flow solution and where x^c , y^c are the cell-centered coordinates of the grid in the domain. The output is given by $\nu_t(\mathbf{x})$ which is the steady-state turbulent eddy viscosity potentially obtained from any choice of RANS closure strategies. We train our ML surrogate given by a neural network with 6 hidden layers and 40 neurons in each layer along with rectified linear activation. In our training procedure we use the ADAM optimizer[22] with a learning rate of 0.001. The fully trained network achieves a coefficient of determination of $R^2 = 0.998^2$ for both training and validation data sets indicating a successful parameterization. The training of the network was terminated using an early-stopping criterion. If validation errors did not improve for 10 epochs, the training would exit with the best model (corresponding to the lowest validation loss until then). We note that the trained framework was deployed with a truncation in case of negative value predictions akin to the built-in limiters of the SA model itself. We note that the hyperparameters of our network and its architecture were hand-tuned for accuracy due to its relative simplicity. Further analysis of this training will be performed in Section 3.1.

3 Results

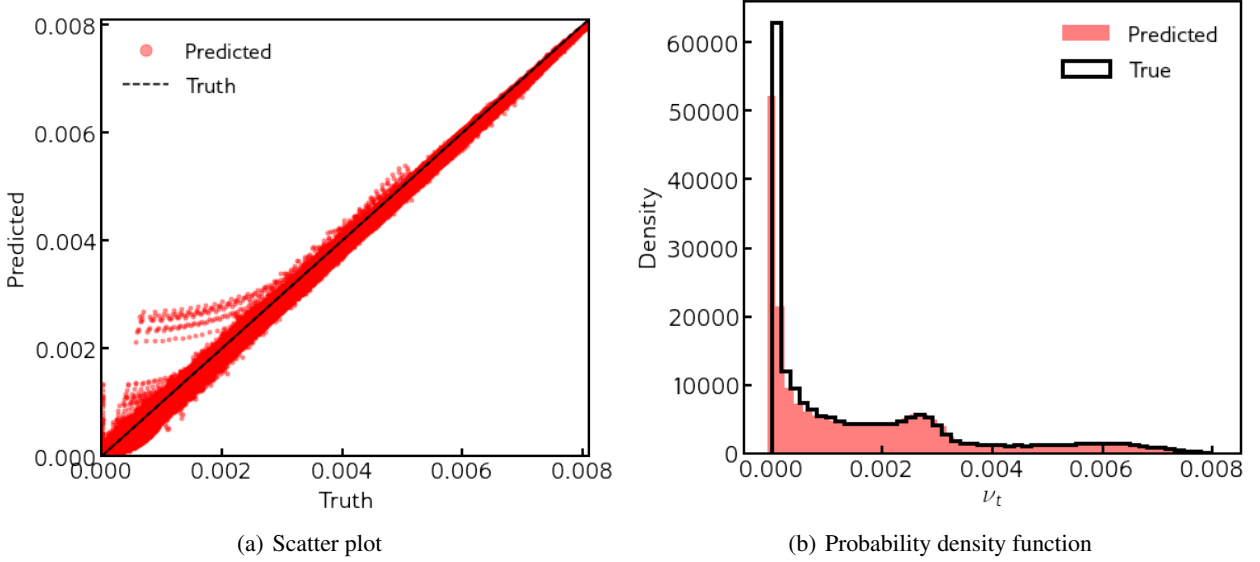
In the following section, we outline our machine learning effectiveness through *a priori* analyses followed by a discussion of the results from its deployment as a surrogate model.

3.1 Machine learning

We proceed by outlining the effectiveness of the machine learning through statistical estimates for its performance. Figure 2 shows the progress to convergence for our learning framework. It was observed that 30 epochs were sufficient for an accurate parameterization of the input-output relationship after which the early-stopping criteria terminated training. The training data set consisted of 205,390 samples corresponding to internal field sampling of inputs and outputs for ten different inlet velocities. Out of the total number of samples 90% were retained for the purpose of training while the rest were utilized for validation.

A statistical assessment of the learning is shown in figure 3. We note that these plots utilize training and validation data for all simulations for the purpose of *a priori* assessment. The scatter plot shows a good agreement between

$$^2 R^2 \equiv 1 - \frac{\sum_i (y_i - y_i^{\text{pred}})^2}{\sum_i (y_i - \bar{y})^2} \text{ for data } y_i, \text{ predictions } y_i^{\text{pred}} \text{ and mean } \bar{y}.$$

Figure 3: An *a priori* statistical assessment of the trained deep learning framework.

Order	1	2	3	4	5	6	7	8	9	10	11	DNN
R^2	0.073	0.264	0.574	0.832	0.915	0.935	0.951	0.955	0.965	0.956	0.692	0.998

Table 2: Validation R^2 values for different order polynomial fits for the proposed training data. The proposed deep learning framework (DNN) is seen to outperform these regressions. It was also observed that RANS deployments did not converge to the preset solver tolerances.

modeled and true magnitudes of ν_t particularly for the higher magnitudes (generally present in the separation zone). Some deviation is observed at the lower magnitudes potentially due to slight inaccuracies in the characterization of the transition from the separation zone to the free-stream. The highest deviations from the truth are observed in the near-wall region of the separated zone as shown later in figure 11. The probability distribution plots for the predicted and true models also show good agreement. We note that the two peaks of the ν_t magnitude are captured accurately by the predictions. As a further exploration of the benefits of using a deep learning framework, the *a priori* performance of the framework is assessed against linear and polynomial regression using the same inputs and output. The R^2 values (for validation data) for these assessments are shown in Table 2. The proposed framework can be seen to outperform the polynomial regression which starts overfitting the training data around an order of 11.

3.2 Surrogate for the Spalart-Allmaras model

In the following section, we outline the results from our proposed formulation for an interpolation task within a range of boundary conditions sampled for training data by the SA turbulence model. We remind the reader that the machine learning framework predicts the steady-state viscosity when the simulation is initialized and the solver then utilizes this fixed viscosity for its progress to convergence. We shall be deploying our proposed framework on two *testing* situations with inlet velocity conditions given by 44.2 m/s (denoted S1) and 49.5 m/s (denoted S2). Both these inlet velocity conditions constitute data that is unseen by the network during training.

Figure 4 shows a line plot for the velocity magnitudes ($|U|$) (for both S1 and S2) at probe location 1 (previously defined in Section 2.1). A close agreement is observed between the converged simulation using the machine learning surrogate and the standard deployment of SA. A strength of this proposed approach is that the velocity and pressure solvers were untouched during our surrogate modeling and the converged fields preserve their respective symmetries. Figure 5 shows the performance of the network in predicting the output quantity (i.e., ν_t) at probe location 1. The spike in the near-wall magnitude of ν_t due to the higher inlet velocity is captured by the training although the transition from the separation zone to the free-stream is slightly erroneous. This may be linked to the larger errors observed at the lower magnitudes of ν_t in figure 3. However, overall trends remain promising.

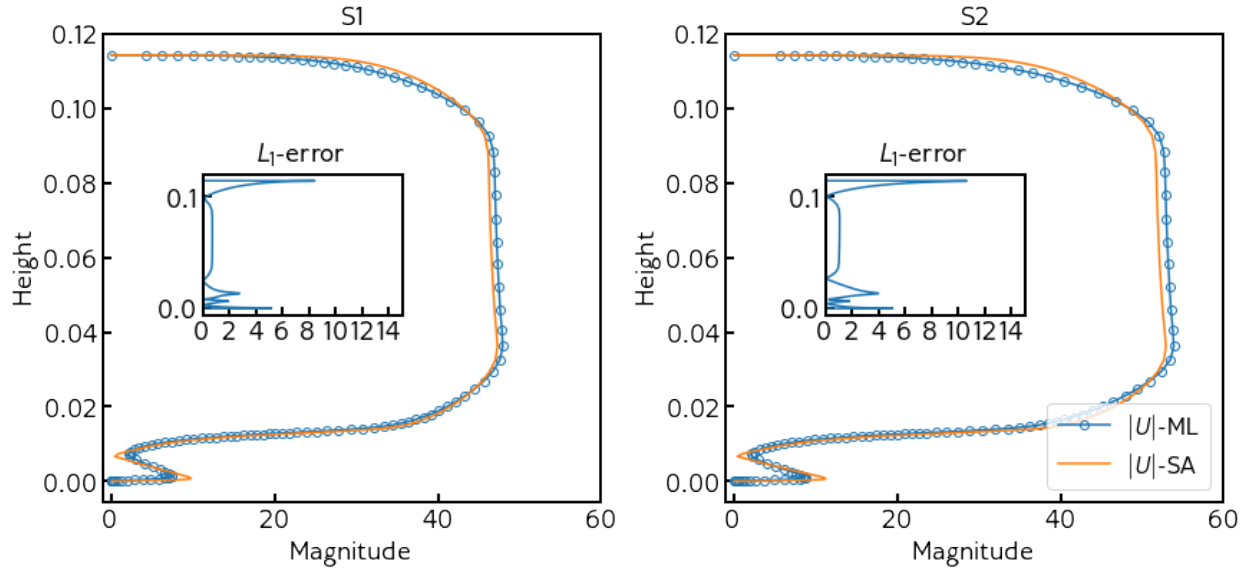


Figure 4: $|U|$ predictions (in m/s) at probe location 1 for surrogate model S1 (left) and S2 (right).

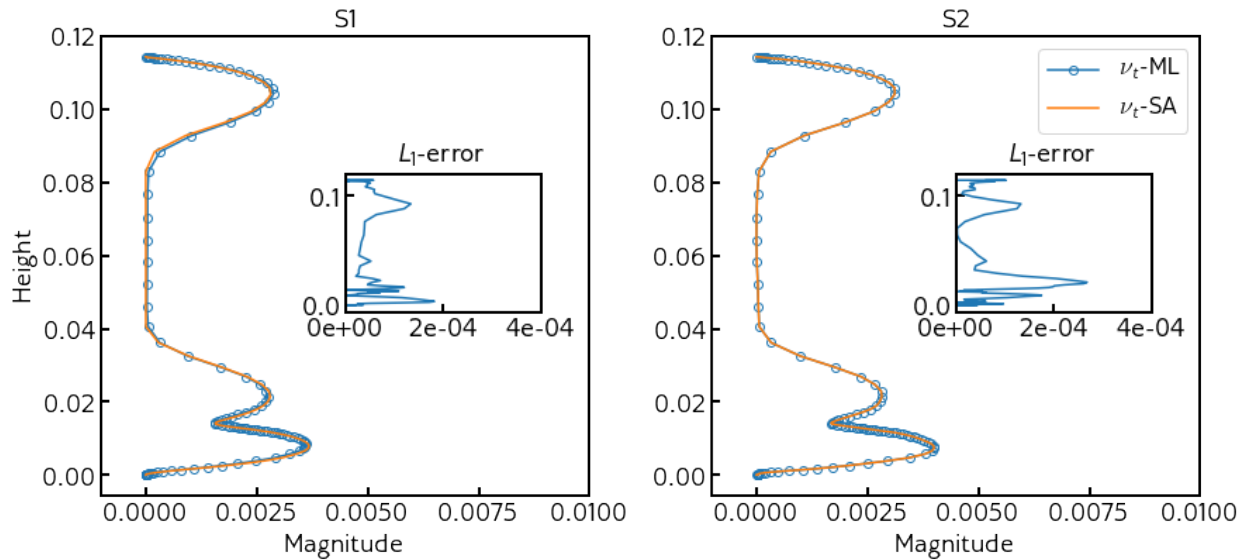


Figure 5: Turbulent eddy-viscosity predictions (in m^2/s) at probe location 1 for surrogate model S1 (left) and S2 (right).

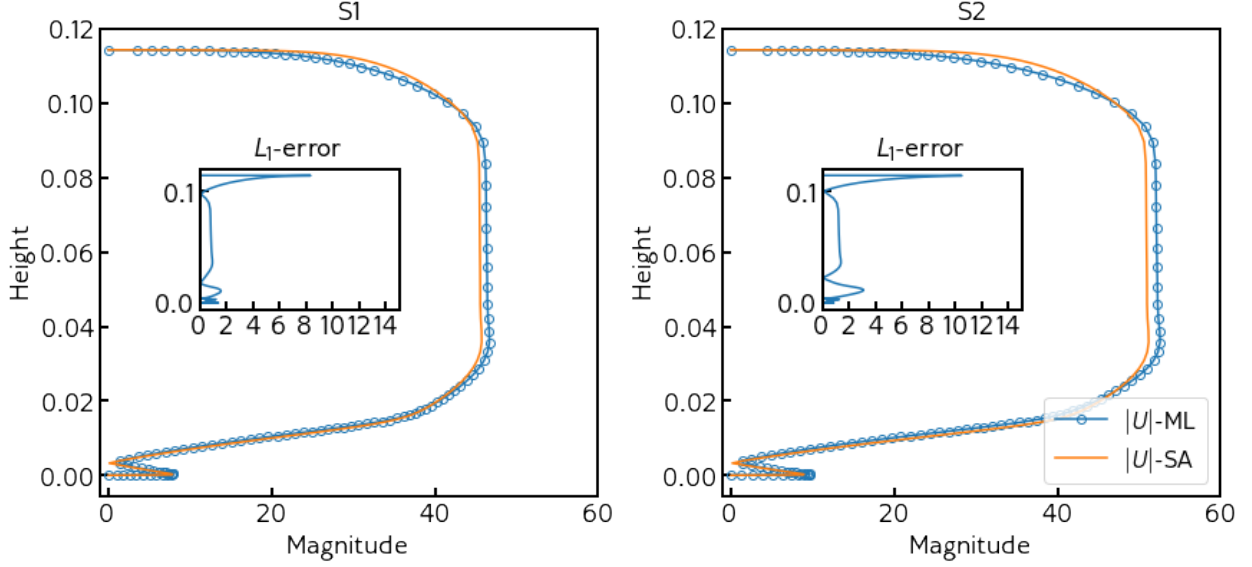


Figure 6: $|U|$ predictions (in m/s) at probe location 2 for surrogate model S1 (left) and S2 (right).

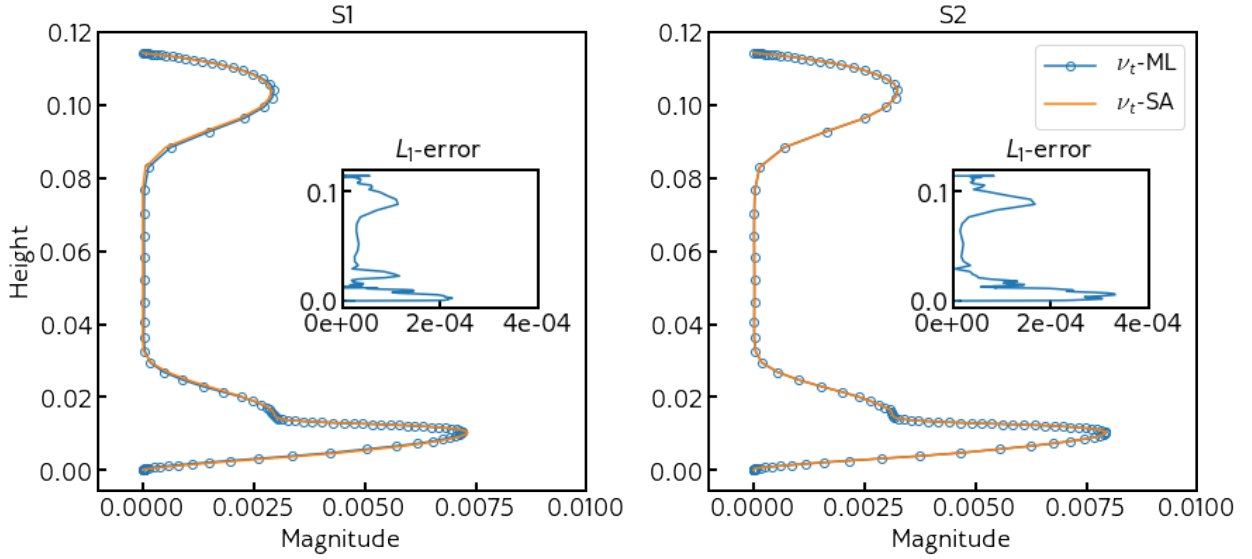


Figure 7: Turbulent eddy-viscosity predictions (in m^2/s) at probe location 2 for surrogate model S1 (left) and S2 (right).

Further assessments of the surrogate are performed for both our testing simulations at different probe locations as shown in figure 6 and figure 7 for the $|U|$ and ν_t further downstream of the step where a good agreement between the one-equation model and the surrogate is once again observed. Our third probe location (located before the flow reaches the step) also shows that the deep learning framework approximates the behavior of SA appropriately as shown in figures 8 and 9. Finally, for a qualitative assessment of the framework, see the contours in figure 10. They show good agreement between predictions and calculations for ν_t and $|U|$ fields. Also, figure 11 shows L_1 errors between truth and prediction where it is observed that errors are an order of magnitude lower than the quantities of interest.

3.3 Speedup from the proposed approach

One of the advantages of the proposed formulation is the removal of an additional PDE for the calculation of $\bar{\nu}$ utilized for specifying ν_t . While one might expect a speedup due to the reduced dimensionality of the coupled PDE system, it is not clear if this would manifest in a reduced time to solution due to the complicated interplay with deep learning

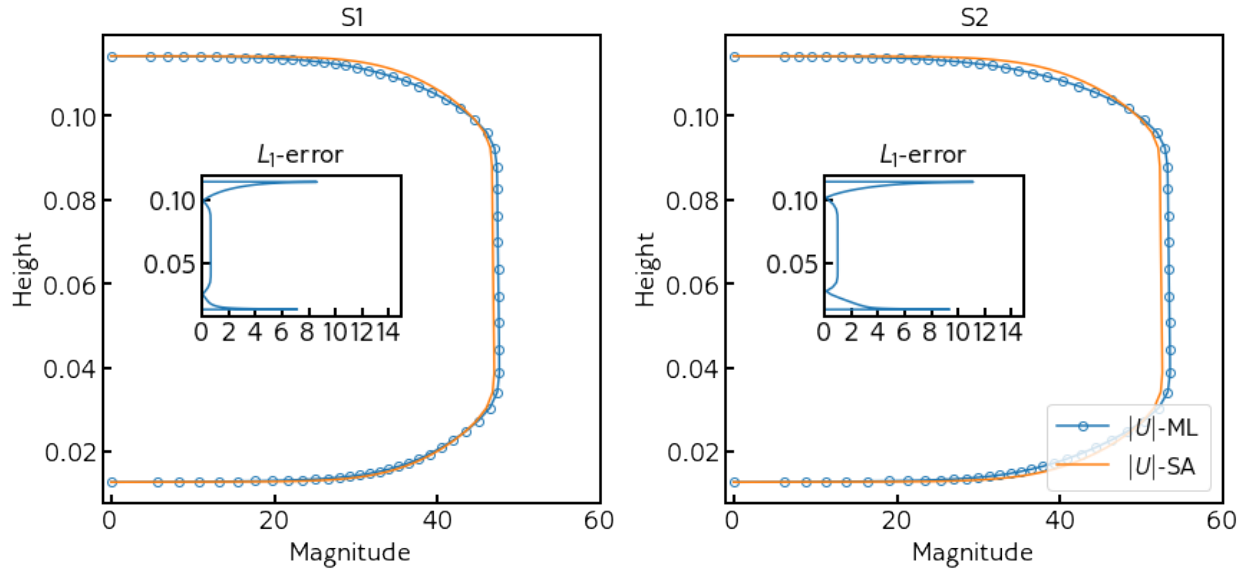


Figure 8: $|U|$ predictions (in m/s) at probe location 3 for surrogate model S1 (left) and S2 (right).

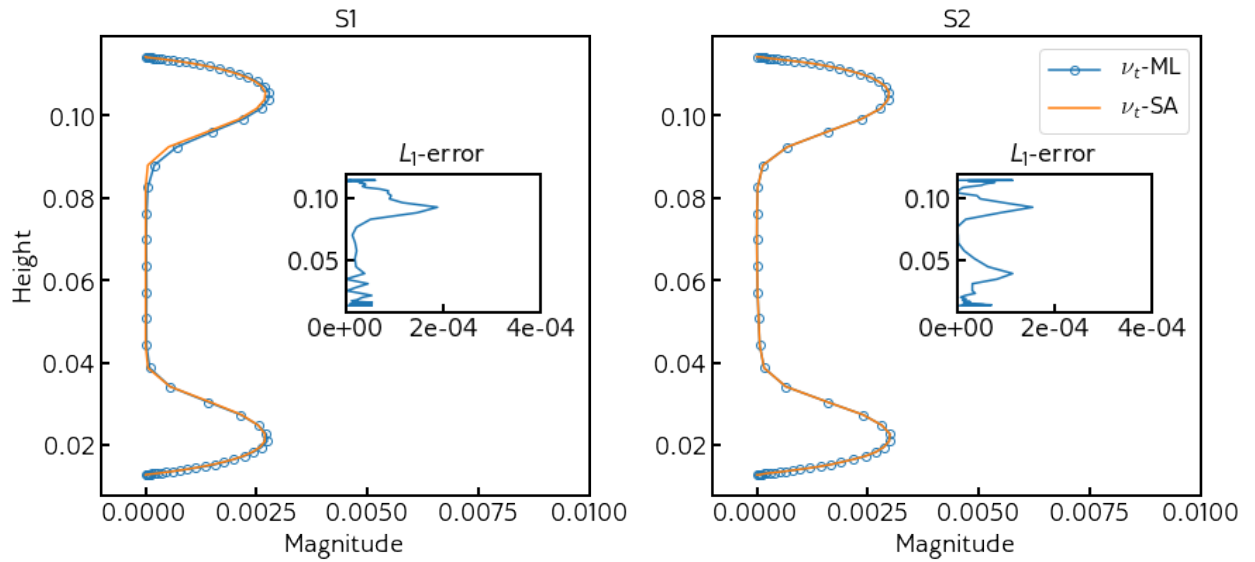


Figure 9: Turbulent eddy-viscosity predictions (in m^2/s) at probe location 3 for surrogate model S1 (left) and S2 (right).

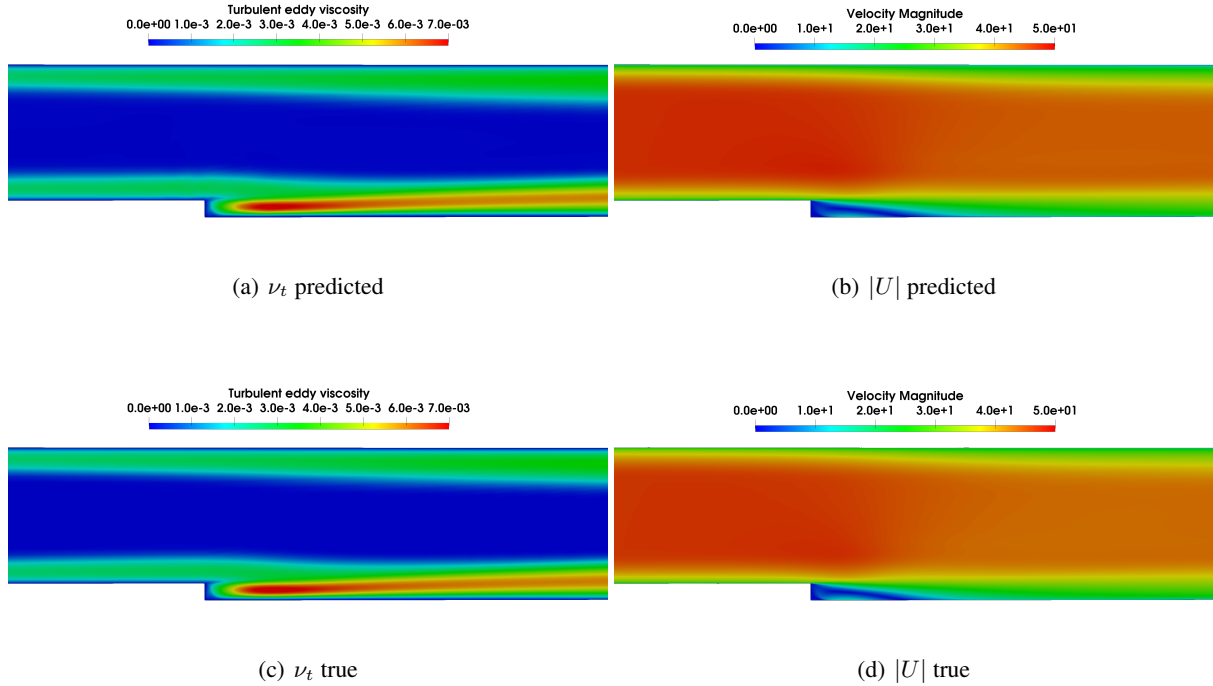


Figure 10: Contour plots for S1. Note that the training set for the ML surrogate did not include this boundary condition.

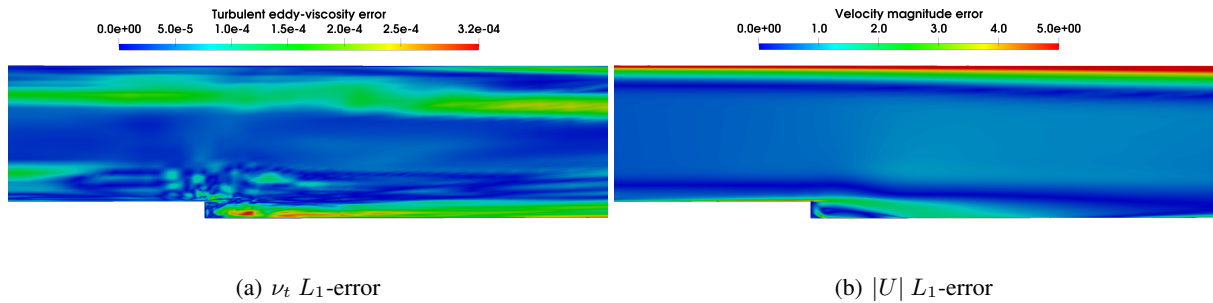


Figure 11: L_1 errors from the ML surrogate for case S1. Errors are concentrated near the region of the step, due to mesh anisotropy. In addition, error spikes are seen on the upper boundary. Note that error magnitudes are an order of magnitude less than the quantities of interest.

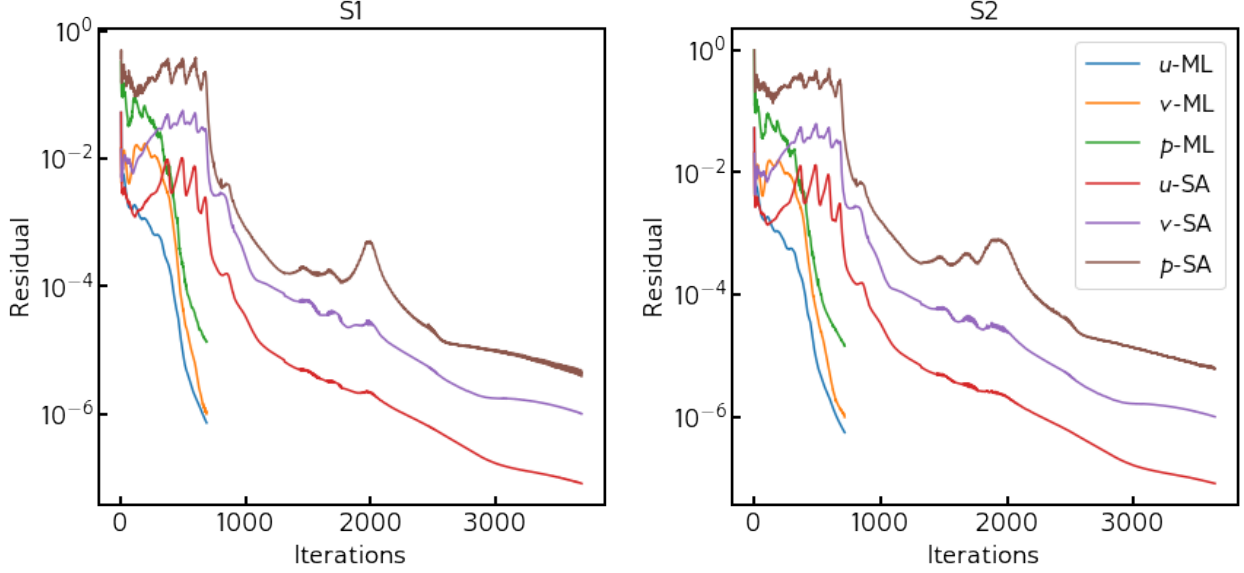


Figure 12: Residual plots for case S1 (left) and S2 (right) exhibiting the speedup from the proposed approach.

prediction errors and the steady-state solvers for velocity and pressure. Through an empirical assessment, we determined that the proposed methodology would allow for considerably *larger* relaxation factors for the steady-state velocity and pressure solvers. In the case of the two surrogate models tested above, relaxation factors of 0.9 each for both pressure and velocity led to a converged solution in 687 iterations of the steady-state solver for S1 and 716 iterations for S2. The SA implementations, however, needed 3696 and 3646 iterations for convergence while utilizing relaxation factors of 0.5 for pressure, 0.9 for velocity and 0.3 for $\bar{\nu}$. We note that the relaxation factors for this deployment were hand-tuned to obtain convergence and that speedup factors are relative. A graphical representation of the speedup is provided in figure 12. In terms of time to solution for experiment S1, the proposed framework required 14.49 seconds for convergence whereas the SA model required 102.76 seconds. For experiment S2, the corresponding times-to-solution were 15.08 and 112.60 seconds. We note that all experiments were performed using a serial execution of OpenFOAM on an Intel Core-i7 processor with a clockspeed of 1.90 GHz.

3.4 Surrogate for two-equation models

To demonstrate the utility of the current machine learning surrogate for turbulent eddy-viscosity models that utilize higher fidelity approximations - we also train the neural network on training data generated from two different two-equation models, namely, the $k - \omega$ SST approximation for ν_t and the RNG $k - \epsilon$ model. We preface our results for this assessment by stating that these demonstrations are performed for training and testing solely on one boundary condition (i.e., inlet velocity) for the purpose of a proof-of-concept. We note that the data for this assessment was generated using first-order upwind methods whereas the SA deployments utilized second-order accurate discretizations. These discretizations were kept consistent for both the training data generation and the surrogate deployments. Figure 13 shows the results of the surrogate modeling framework for the two additional turbulence modeling strategies. While the ML surrogate captures the near wall trends of the velocity profile well for the former, slight inaccuracies are observed for the those of the latter potentially due to the fact that first-order methods may amplify smaller errors in ν_t . We note that despite the use of lower-order methods in the training data generation which led to a reduced number of iterations for convergence (871 and 990 iterations respectively for $k - \omega$ SST and $k - \epsilon$ RNG), the deployment of the ML surrogate required 384 and 396 iterations respectively. This indicated a considerable acceleration as well.

4 Conclusion & Future work

This investigation outlines results from the development of a machine learning framework that converts the RANS closure problem to an interpolation task through the integration of machine learning. Our proposed formulation utilizes a neural network surrogate model that is trained on data generated by sampling a region in parameter space and which is deployed in the vicinity of this space for instant prediction of steady-state turbulent eddy-viscosity profiles. The inputs

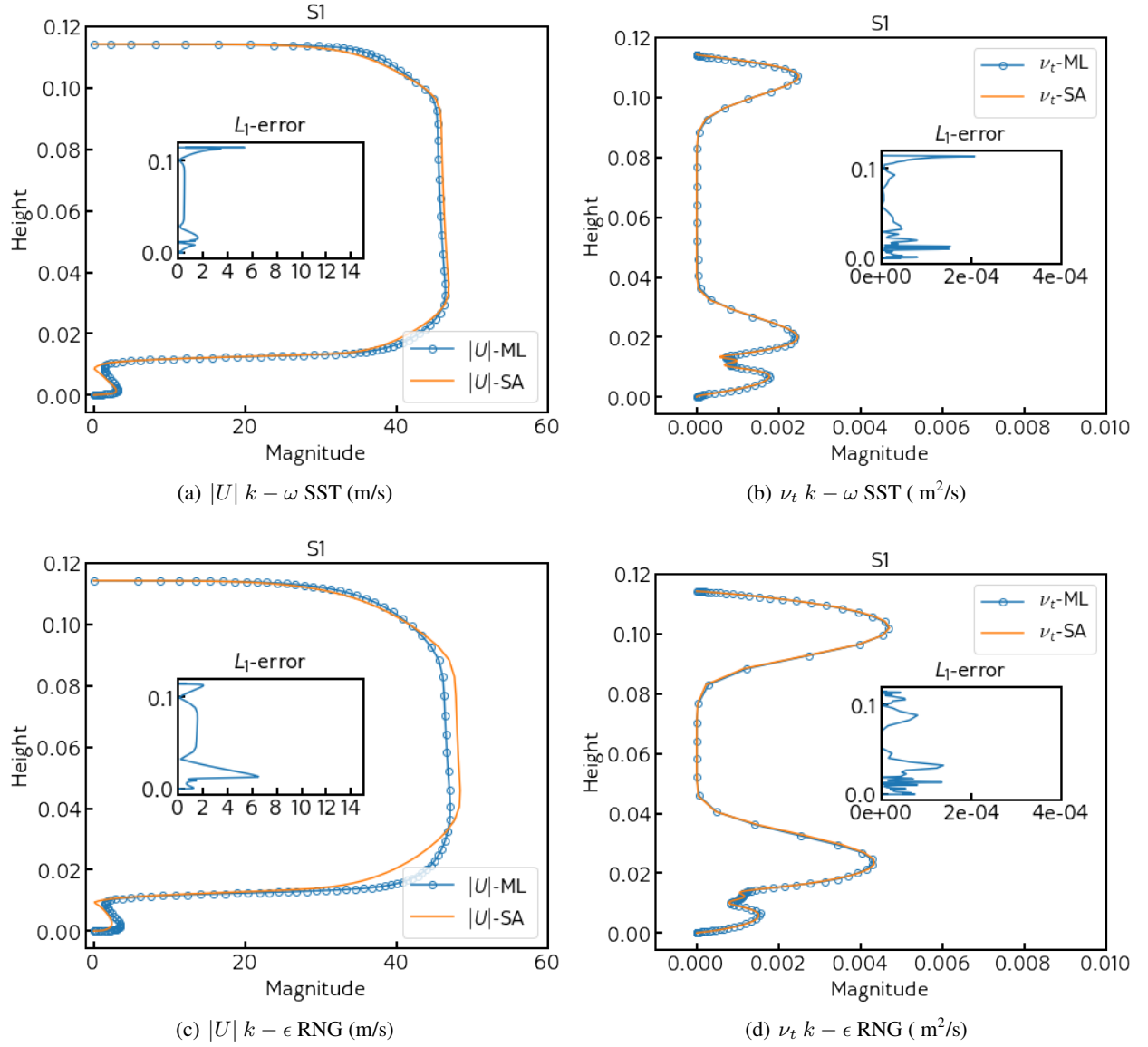


Figure 13: Surrogate modeling results for the training data generated from different closures with $k - \omega$ SST (top) and $k - \epsilon$ RNG (bottom) showing the ability of the proposed framework to reconstruct higher fidelity fields at probe location 1. It is observed that the slight errors in the ν_t profile for the RNG model have an effect on the $|U|$ prediction.

to the deep learning framework are given by a potential flow solution to the internal flow. The framework is tested by providing surrogates to the SA, $k - \omega$ SST, and $k - \epsilon$ RNG turbulence closures for a two-dimensional backward-facing step problem and leads to an accurate reconstruction of steady-state solutions. The errors associated with our quantities of interest are an order of magnitude lower than their maximum field values when deploying the ML surrogate. The preclusion of an additional set of equations for turbulent eddy-viscosity calculation also leads to a significant reduction in the time to solution for the RANS problem using a surrogate closure. Times-to-solution for the ML framework are approximately 7 times lower for an ML surrogate trained on the SA equation which utilized central schemes for its discretization while a speed-up factor of approximately 2 was obtained for the two-equation models which used first-order upwinding for the advective term. In the case of the one-equation SA model, the framework is also tested for interpolation within a sampled region which leads to accurate results for unseen initial conditions as well. We note that the formulation avoids any modification to the velocity and pressure solvers thereby leading to the preservation of the symmetries of the steady-state RANS equations.

The conclusions from this investigation suggest the feasibility of building surrogates for sub-grid quantities for statistically steady-state problems using high-fidelity methods such as LES. Further investigation into physics regularized optimization of the steady-state mapping procedure (for instance to ensure alignment with our understanding of sub-grid mathematical properties) is also underway for greater confidence in the neural network predictions. While the current study utilizes uniformly spaced samples for different inlet velocities for training data set generation, greedy sampling strategies may be incorporated into the proposed workflow for sampling from a higher-dimensional control parameter space. The current results suggest that effective surrogate building of turbulence closure quantities using an ML framework can shift a large proportion of the online cost of parameter space exploration for assessing design quantities of interest to an offline sampling of the parameter space.

Acknowledgments

This material is based upon work supported by the U.S. Department of Energy (DOE), Office of Science, Office of Advanced Scientific Computing Research, under Contract DE-AC02-06CH11357. This research was funded in part and used resources of the Argonne Leadership Computing Facility, which is a DOE Office of Science User Facility supported under Contract DE-AC02-06CH11357. This paper describes objective technical results and analysis. Any subjective views or opinions that might be expressed in the paper do not necessarily represent the views of the U.S. DOE or the United States Government.

References

- [1] Julia Ling and J Templeton. Evaluation of machine learning algorithms for prediction of regions of high Reynolds averaged Navier Stokes uncertainty. *Phys. Fluids*, 27(8):085103, 2015.
- [2] Julia Ling, Andrew Kurzwaski, and Jeremy Templeton. Reynolds averaged turbulence modelling using deep neural networks with embedded invariance. *J. Fluid Mech.*, 807:155–166, 2016.
- [3] Jin-Long Wu, Heng Xiao, and Eric Paterson. Physics-informed machine learning approach for augmenting turbulence models: A comprehensive framework. *Phys. Rev. Fl.*, 3(7):074602, 2018.
- [4] Eric J Parish and Karthik Duraisamy. A paradigm for data-driven predictive modeling using field inversion and machine learning. *J. Comp. Phys.*, 305:758–774, 2016.
- [5] R Matai and PA Durbin. Zonal eddy viscosity models based on machine learning. *Flow, Turbulence and Combustion*, 103(1):93–109, 2019.
- [6] Romit Maulik, Omer San, Jamey D Jacob, and Christopher Crick. Sub-grid scale model classification and blending through deep learning. *J. Fluid Mech.*, 870:784–812, 2019.
- [7] Masataka Gamahara and Yuji Hattori. Searching for turbulence models by artificial neural network. *Phys. Rev. Fl.*, 2(5):054604, 2017.
- [8] Romit Maulik and Omer San. A neural network approach for the blind deconvolution of turbulent flows. *J. Fluid Mech.*, 831:151–181, 2017.
- [9] Antoine Vollant, Guillaume Balarac, and C Corre. Subgrid-scale scalar flux modelling based on optimal estimation theory and machine-learning procedures. *J. Turbul.*, 18(9):854–878, 2017.
- [10] Kai Fukami, Koji Fukagata, and Kunihiro Taira. Super-resolution reconstruction of turbulent flows with machine learning. *J. Fluid Mech.*, 870:106–120, 2019.

- [11] Karthik Duraisamy, Gianluca Iaccarino, and Heng Xiao. Turbulence modeling in the age of data. *Annu. Rev. Fluid Mech.*, 51:357–377, 2019.
- [12] Linyang Zhu, Weiwei Zhang, Jiaqing Kou, and Yilang Liu. Machine learning methods for turbulence modeling in subsonic flows around airfoils. *Phys. Fluids*, 31(1):015105, 2019.
- [13] David M Driver and H Lee Seegmiller. Features of a reattaching turbulent shear layer in divergent channel flow. *AIAA J.*, 23(2):163–171, 1985.
- [14] Henry G Weller, Gavin Tabor, Hrvoje Jasak, and Christer Fureby. A tensorial approach to computational continuum mechanics using object-oriented techniques. *Comput. Phys.*, 12(6):620–631, 1998.
- [15] E Robertson, V Choudhury, S Bhushan, and DK Walters. Validation of OpenFOAM numerical methods and turbulence models for incompressible bluff body flows. *Comput. Fluids*, 123:122–145, 2015.
- [16] Osborne Reynolds. IV. On the dynamical theory of incompressible viscous fluids and the determination of the criterion. *Philos. Trans. R. Soc. London, Ser. A*, (186):123–164, 1895.
- [17] P Yo Chou. On velocity correlations and the solutions of the equations of turbulent fluctuation. *Q. Appl. Math.*, 3(1):38–54, 1945.
- [18] Philippe Spalart and Steven Allmaras. A one-equation turbulence model for aerodynamic flows. In *30th aerospace sciences meeting and exhibit*, page 439, 1992.
- [19] VSASTBCG Yakhot, SA Orszag, Siva Thangam, TB Gatski, and CG Speziale. Development of turbulence models for shear flows by a double expansion technique. *Phys. Fluids*, 4(7):1510–1520, 1992.
- [20] Florian R Menter. Two-equation eddy-viscosity turbulence models for engineering applications. *AIAA J.*, 32(8):1598–1605, 1994.
- [21] Martín Abadi, Ashish Agarwal, Paul Barham, Eugene Brevdo, Zhifeng Chen, Craig Citro, Greg S. Corrado, Andy Davis, Jeffrey Dean, Matthieu Devin, Sanjay Ghemawat, Ian Goodfellow, Andrew Harp, Geoffrey Irving, Michael Isard, Yangqing Jia, Rafal Jozefowicz, Lukasz Kaiser, Manjunath Kudlur, Josh Levenberg, Dandelion Mané, Rajat Monga, Sherry Moore, Derek Murray, Chris Olah, Mike Schuster, Jonathon Shlens, Benoit Steiner, Ilya Sutskever, Kunal Talwar, Paul Tucker, Vincent Vanhoucke, Vijay Vasudevan, Fernanda Viégas, Oriol Vinyals, Pete Warden, Martin Wattenberg, Martin Wicke, Yuan Yu, and Xiaoqiang Zheng. TensorFlow: Large-scale machine learning on heterogeneous systems, 2015. Software available from tensorflow.org.
- [22] Diederik P Kingma and Jimmy Ba. Adam: A method for stochastic optimization. *arXiv preprint arXiv:1412.6980*, 2014.